JMEPEG (2009) 18:1073–1077
DOI: 10.1007/s11665-008-9337-y

1059-9495/$19.00

Mechanical Properties of Ternary Sn-In-Ag Ball-Grid Array Assemblies at Ambient and Elevated Temperatures

M.S. Yeh and J.T. Chiang

(Submitted October 23, 2007; in revised form November 20, 2008)

The mechanical behavior of a ternary Sn-15In-2.8Ag ball-grid array assembly was evaluated at ambient and elevated temperatures. The maximum stress of the Sn-15In-2.8Ag ball-grid array assembly decreased as the temperatures increased and the strain rates decreased. An irregular brittle NiSnIn intermetallic layer formed at the SnInAg/Au/Ni/Cu interface, resulting in decreased bond strength of the joints. The Arrhenius diagram of the Sn-15In-2.8Ag ball-grid array assembly at a constant stress of 16 MPa consists of two straight lines intersecting at 50 °C, which indicates that two kinds of creep mechanism controlled the Sn-15In-2.8Ag ball-grid array assembly deformation. The $AuIn_2$ intermetallics and grain boundaries acted as the location for nucleation of the creep voids, which induced reduction of the solder's cross-sectional area and led the Sn-15In-2.8Ag ball-grid array assembly to fail rapidly with a transgranular creep fracture.

Keywords ball-grid array assembly, creep fracture, intermetallic layer, IR reflow process, Sn-15In-2.8Ag solder

1. Introduction

The ball-grid array (BGA) package is a suitable method for manufacturing high input/output interconnect assemblies in the electronic packaging industry. In the BGA packaging, the Au/Ni surface finish is widely used on the contact pads for the solder balls. The surface layer Au is for the oxidation protection and the layer Ni is a diffusion barrier to protect Cu form reacting with Sn. Since the banning of Pb due to environmental and health hazards, several Pb-free solders have been considered as alternatives to Pb-Sn solders (Ref 1, 2). The binary Sn-3.5Ag eutectic alloy is the most attractive solder for the electronics industry, which provides better mechanical properties than those of the Pb-Sn eutectic alloy (Ref 3, 4). However, the Sn-3.5Ag solder possesses a higher melting temperature than that of the Sn-37Pb eutectic solder. The reason restricted its applications in electronic packaging when using the conventional reflow soldering methods. Moreover, the gold embrittlement is still another important reliability issue for BGA applications (Ref 5). Even the failure mode for solder joints has been reported about at least four decades.

Indium is a metal with a low melting point, which could depress the melting temperature of a Sn-Ag alloy. Another advantage of using the indium-containing solder is that the Au dissolves much more slowly into the solder to eliminate the gold embrittlement problem associated with BGA packages (Ref 6). For this reason, the ternary Sn-In-Ag solders would become additional potential replacements for the traditional Pb-Sn solders. In this study, the mechanical behavior of a ternary Sn-15In-2.8Ag BGA assembly was evaluated by tensile testing at ambient and elevated temperatures. Also, the effects of intermetallics were investigated at the interface between the solder and the Au/Ni/Cu pad.

M.S. Yeh and **J.T. Chiang**, Department of Mechanical Engineering, Chung Hua University, 707, Sec. 2, Wu Fu Rd., Hsin Chu 300, Taiwan, ROC. Contact e-mail: ming@chu.edu.tw.

2. Experimental

The ternary Sn-15In-2.8Ag solder was prepared by melting pure metals (99.99 wt.%) into a 100-g ingot within a quartz tube at 600 °C for 12 h, and then the alloy was homogenized at 95 °C for 100 h. Its melting characteristics were determined by differential scanning calorimetry (DSC) under a nitrogen atmosphere with a heating rate of 10 °C/min.

The Sn-15In-2.8Ag ingot was rolled into 0.15-mm-thick sheets and punched to 400 ± 20 μm diameter plates. Twenty-five Sn-15In-2.8Ag plates with BF31 flux were attached to Au/Ni/Cu pads on a printed circuit board (PCB), which was made of $7 \times 7 \times 1$ FR-4 epoxy/glass (Fig. 1). The surface layers Au (0.6 μm) and Ni (5 μm) are deposited by electroplating. Figure 2 shows the infrared (IR) reflow temperature profile and the reflow time is determined by measuring the dwell time above 196.4 °C. The shear (push) force of the Sn-In-Ag solder balls was measured on a Dage automated test machine at a speed of 100 μm/s with the shear blade tip 25 μm from the device planar surface. The interfacial microstructures of the solder/pad were observed with a scanning electron microscope (SEM). Tensile tests were performed using a mechanical testing machine (Instron's model 3365) in air at a strain rate range from 10^{-4} to 10^{-6} s^{-1} at various temperatures. Creep tests were performed at a constant stress over the range 4 to 20 MPa at the deformation temperatures 25, 50, 75, and 100 °C. The temperature chamber was capable of maintaining a constant temperature within

±1 °C. A linear variable differential transformer (LVDT) with a resolution of 0.01 μm was mounted on the BGA samples to measure displacement. An SEM with X-ray dispersive analysis was used to examine the fracture surfaces of both the solder ball side and PCB side after these tests.

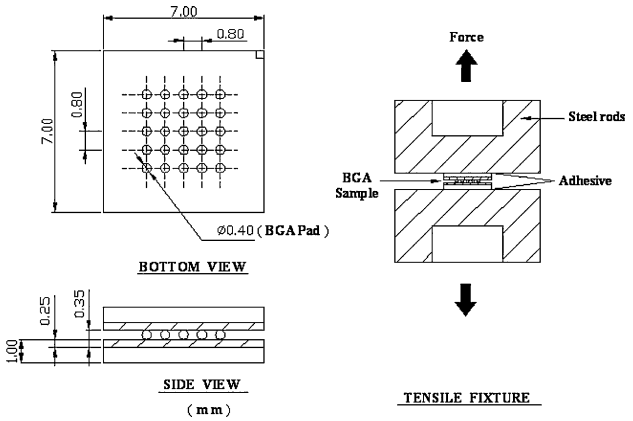

Fig. 1 Geometry and dimensions of BGA specimens for tensile tests

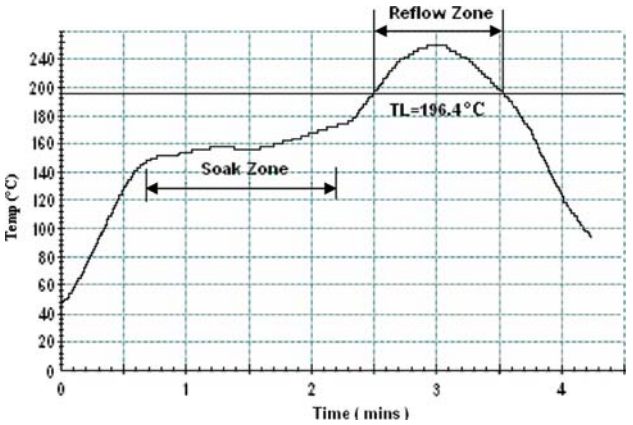

Fig. 2 The reflow temperature profile of the Sn-15In-2.8Ag ball-grid array on PCB

3. Results and Discussion

The melting characteristics of the Sn-15In-2.8Ag solder were determined by DSC. An endothermic peak appeared between 186.6 and 205.1 °C corresponding to its solidus and liquidus (Ref 7), respectively. The cross-sectional interface microstructure between the SnInAg solder ball and the Au/Ni/Cu pad after the IR reflow process is shown in Fig. 3. All the Au thin film disappeared from the interface and reacted with SnInAg solder after the reflow process. An irregular NiSnIn intermetallic layer was found at the SnInAg/Ni/Cu interface. The average thickness of the NiSnIn intermetallic layer was about 3 μm. Some $AuIn_2$ intermetallics were also observed in the Sn matrix.

According to the JEDEC Standard No. 22B117A, the shear tool standoff should be no greater than 25% of the solder ball height. In this study, the shear (push) force of the Sn-In-Ag solder balls was measured on a Dage automated test machine at a speed of 100 μm/s with the shear blade tip 25 μm from the device planar surface. The shear force was about 4.83 ± 0.55 N. The failure location was in the bulk solder material and not at the solder/intermetallic interface (Fig. 4).

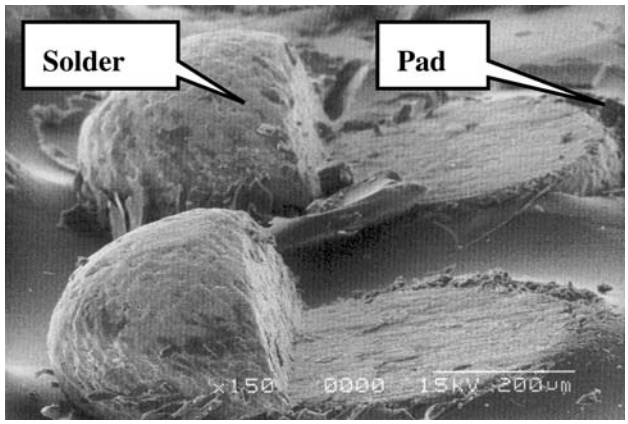

Fig. 4 SEM fractured surface of the Sn-15In-2.8Ag solder ball after shear test

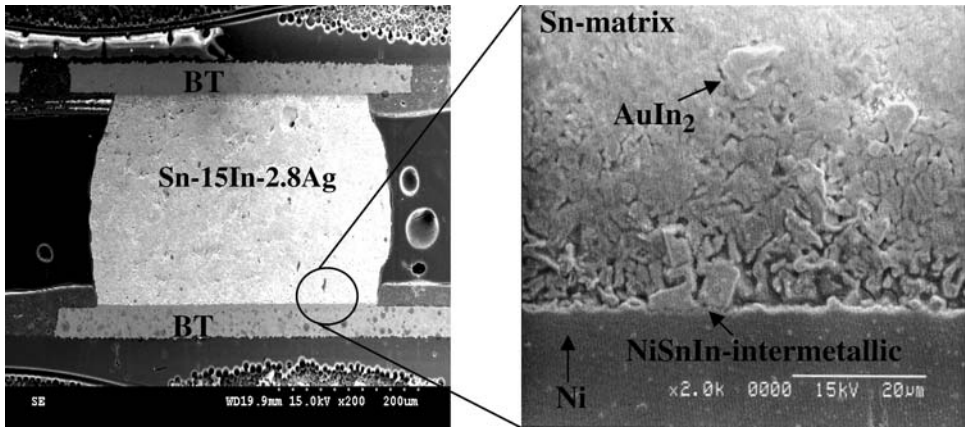

Fig. 3 Cross section of the Sn-15In-2.8Ag BGA assembly

Figure 5 shows the tensile stress-strain curves of the Sn-15In-2.8Ag BGA assembly at a strain rate range from 10^{-4} to 10^{-6} s^{-1} at various temperatures. All tensile data reported are given as:

$$\sigma = \frac{F}{A}; \quad \varepsilon = \frac{\delta}{h}$$

where σ is the average stress per solder joint, F the total applied load, A the total pad area, ε the strain, δ the displacement, and h is the joint height. The maximum stress of the Sn-15In-2.8Ag BGA assembly at a strain rate of 10^{-4} s^{-1} decreased from 32.4 to 18.1 MPa as the test temperatures increased from room temperature to 100 °C. The flow stresses of the Sn-15In-2.8Ag BGA assembly decreased as the test temperatures increased and the testing strain rates decreased.

The strain rates and test temperatures could affect the fracture mode of the Sn-15In-2.8Ag BGA assembly during the tensile tests. Figure 6 shows the typical fracture surfaces of Sn-15In-2.8Ag solder joint failure in the BGA assembly at various testing conditions. Top of the figure shows the ball side and bottom the chip side. The cracks first nucleate at the SnInAg/Ni/Cu interfaces due to tensile stress, and then propagate along a 45° angle with the tensile axis at strain rates higher than 10^{-4} s^{-1} and/or at test temperatures lower than 50 °C (Fig. 6a-c). This implies that the brittle NiSnIn intermetallic layer decreased the bond strength on the SnInAg/Ni/Cu interface. The fracture surface of this assembly was of the mixed-mode type, having both brittle and ductile components. However, when the assembly was tested at strain rates lower than 10^{-4} s^{-1} or at test temperatures higher than 75 °C, the ductile fracture mode became dominant, resulting in the cup-and-cone configuration (Fig. 6d-f). The BGA assemblies all failed in the solder balls, not at the interfaces between the solder and Au/Ni/Cu pad even with a brittle NiSnIn intermetallic layer.

The Sn-15In-2.8Ag solder possesses a melting range between 186.6 and 205.1 °C; this indicates that creep effect plays a very important deformation role even at room temperature. Figure 7 shows the schematic creep curves of the Sn-15In-2.8Ag BGA assemblies. The relationship between applied stress and strain rate can be represented by the power law:

$$\dot{\varepsilon} = A\sigma^n \exp\left[\frac{-Q}{RT}\right]$$

where $\dot{\varepsilon}$ is the minimum creep rate, A is a constant, σ the applied stress, Q the activation energy for creep, R the universal gas constant (8.3144 J/mol K), T the absolute temperature, and n is the stress exponent. Mavoori et al. (Ref 4) reported that a stress exponent of 3-4 indicated viscous dislocation glide control for creep. If the value of n is equal to 6-7, the creep-controlling mechanism is intergranular dislocation climb. Figure 8 shows the relationship between the minimum creep rate and the stress on a double-logarithmic scale. The Arrhenius diagrams for the Sn-15In-2.8Ag BGA assemblies under various constant stresses are also shown in Fig. 9. All the data were determined by calculating the average from three specimens. A stress exponent of 3.6-4.2 and apparent activation energies of the Sn-15In-2.8Ag BGA assembly which varied from 46.1 to 53.2 kJ/mol were obtained under applied stress below 12 MPa. The activation energies were very close to 0.7 times that of pure tin ($Q_c = 60.3 \pm 3.87$ kJ/mol) (Ref 8). Upon comparing the stress exponent and activation

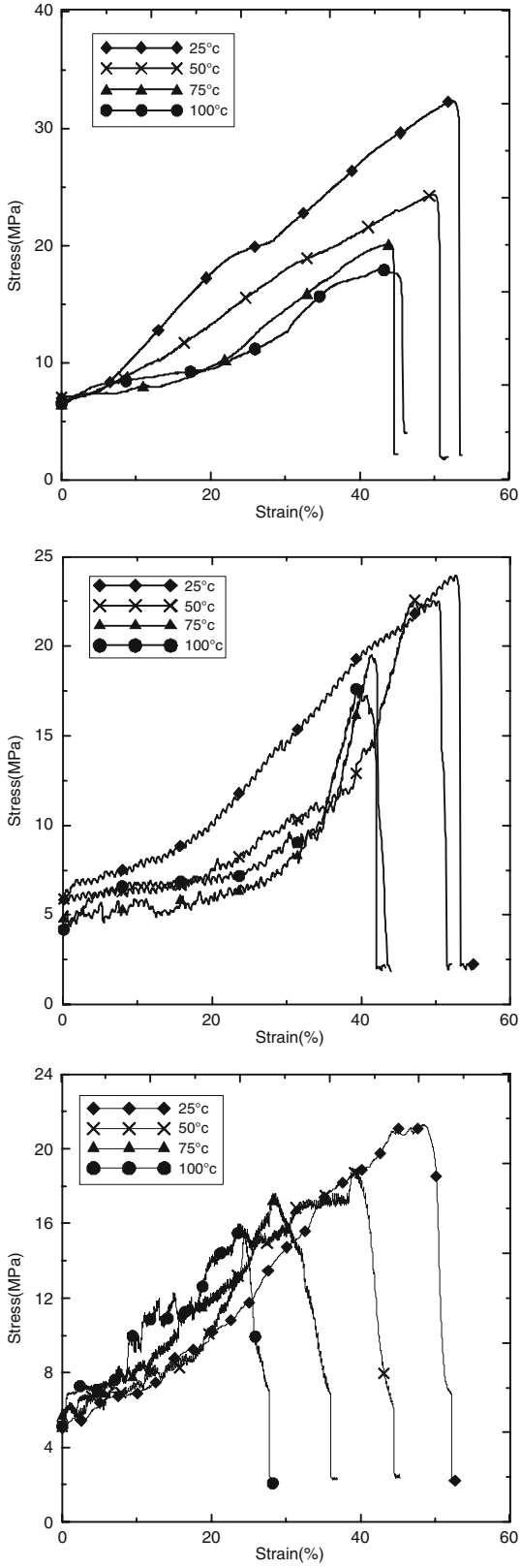

Fig. 5 The σ-ε curves of Sn-15In-2.8Ag BGA assembly at a strain rate range from 10^{-4} to 10^{-6} s^{-1} at various temperatures: (a) 10^{-4} s^{-1}, (b) 10^{-5} s^{-1}, and (c) 10^{-6} s^{-1}

energies obtained in this study with those for pure tin, the viscous glide appears to be the creep-controlling deformation mechanism in the lower stress region. On the other hand,

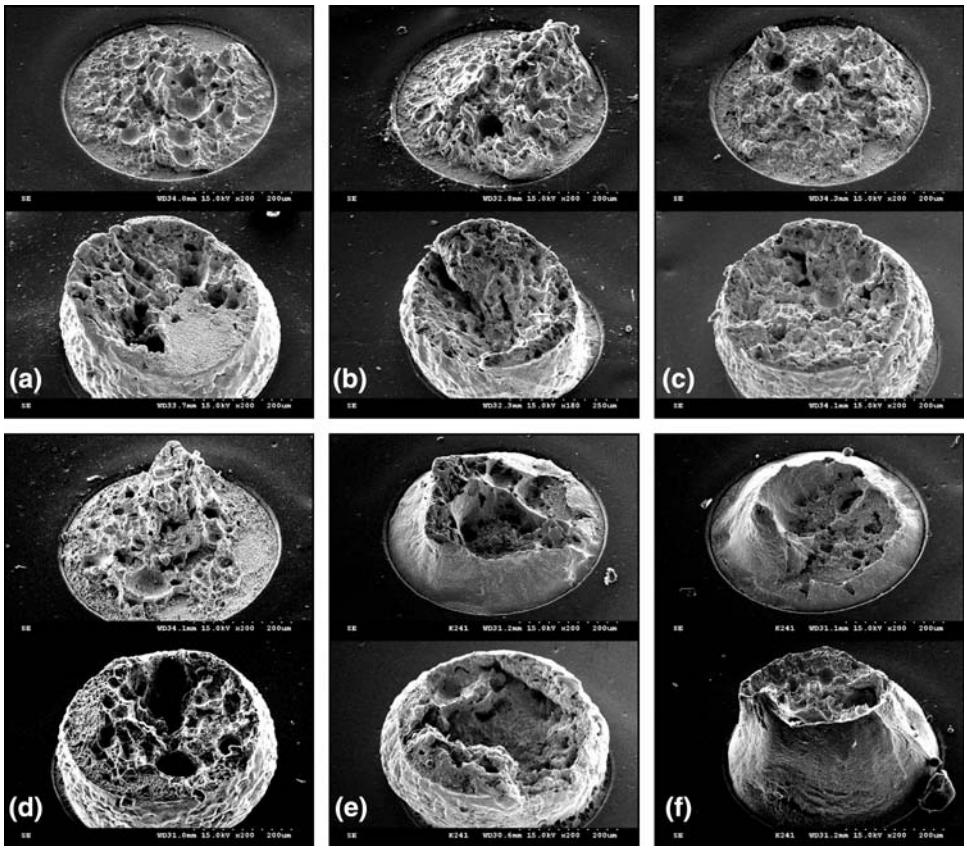

Fig. 6 The Sn-15In-2.8Ag solder joint failures in the BGA assembly at various testing conditions: (a) 10^{-4} s^{-1}, 25 °C, (b) 10^{-4} s^{-1}, 100 °C, (c) 10^{-5} s^{-1}, 50 °C, (d) 10^{-5} s^{-1}, 100 °C, (e) 10^{-6} s^{-1}, 75 °C, and (f) 10^{-6} s^{-1}, 100 °C

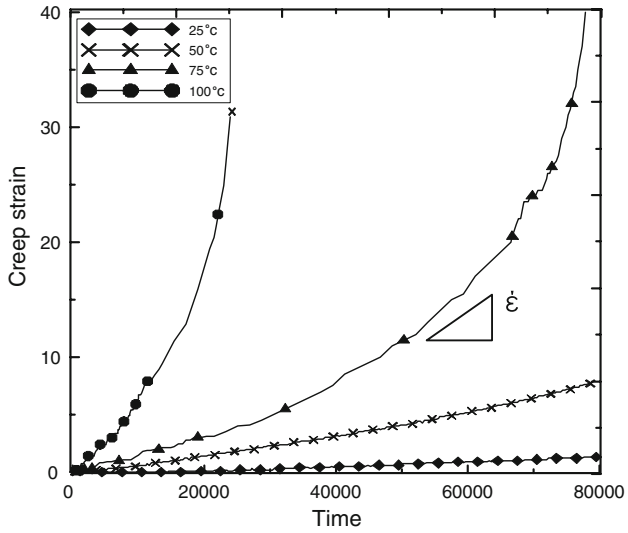

Fig. 7 Schematic creep curves of the Sn-15In-2.8Ag ball-grid array assemblies under constant stress at various temperatures

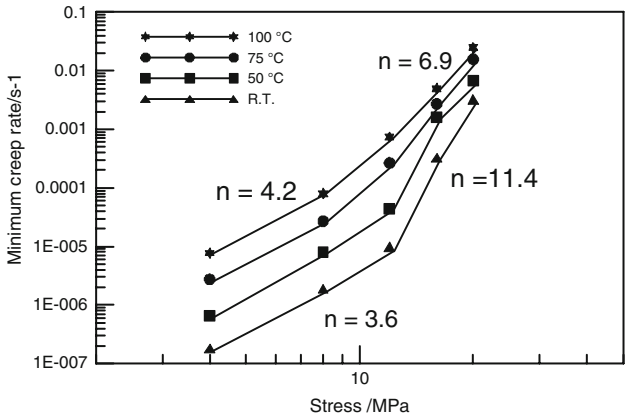

Fig. 8 The relationship between the minimum creep rate and the stress on double-logarithmic scale

the Sn-15In-2.8Ag alloy is similar to the Sn-3.5Ag alloy, which is strengthened by the Ag_3Sn intermetallics. Higher stress exponents of 6.9-11.4 were obtained in the high stress regime. Darveaux (Ref 9) has reported that the stress exponents of 5.5 and activation energy for creep of 38 kJ/mol are obtained for the Sn-3.5Ag alloy within the temperature range of 300-405 K. The creep-controlling mechanism was attributed to the dislocation climb. The Arrhenius diagram of the Sn-15In-2.8Ag BGA assembly at constant stress of 16 MPa consists of two straight lines intersecting at 50 °C. The apparent activation energy for creep was 56.1 kJ/mol at a constant stress of 16 MPa at temperatures lower than 50 °C. At higher temperatures, the apparent activation energy for creep was about 24.3 kJ/mol. We would expect there to be a critical temperature for the creep-controlling mechanism to transition

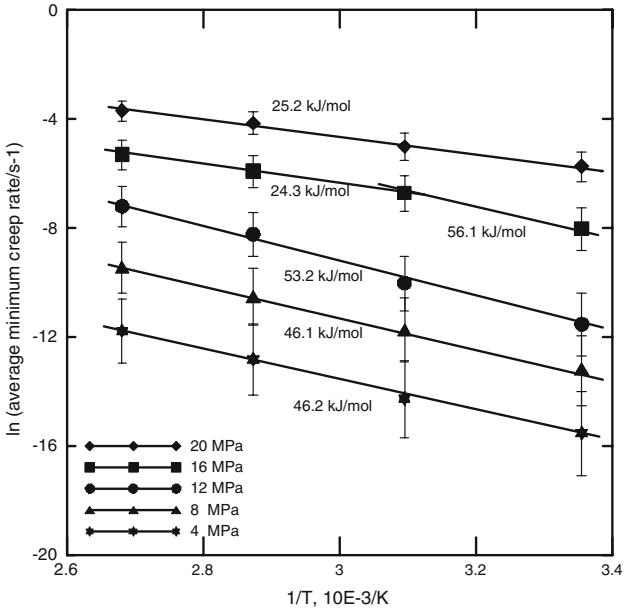

Fig. 9 The Arrhenius diagrams for the Sn-15In-2.8Ag ball-grid array assemblies under various constant stresses

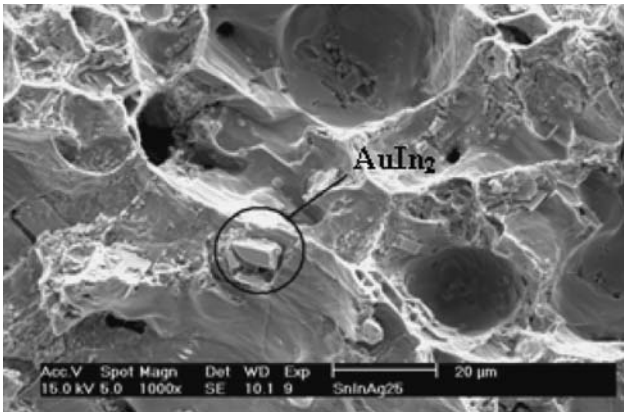

Fig. 10 The $AuIn_2$ intermetallics were observed on typical irregular creep fracture surface of Sn-15In-2.8Ag BGA assembly

from viscous glide creep to dislocation climb. The lower activation energy may be due to the fact that dislocation climb became easier at high temperatures. Many internal voids and $AuIn_2$ intermetallics could be observed on the typical irregular fracture surface (Fig. 10). This might indicate that the voids nucleated at $AuIn_2$ intermetallics or grain boundaries, and then grew by grain-boundary creep diffusion. Finally, the void coalescence led to a reduction in the solder's cross-sectional area, at which point the Sn-15In-2.8Ag BGA assembly failed rapidly with a transgranular creep fracture.

4. Conclusion

After the IR reflow process, an irregular NiSnIn intermetallic layer formed at the interface between the Sn-In-Ag solder and the Au/Ni/Cu contact pads, and $AuIn_2$ intermetallics were observed in the Sn matrix. The shear (push) force of the Sn-In-Ag solder balls was about 4.83 ± 0.55 N. The maximum stress of the Sn-15In-2.8Ag BGA assembly at a strain rate of 10^{-4} s^{-1} decreased from 32.4 to 18.1 MPa as the test temperatures increased from room temperature to 100 °C. The brittle NiSnIn intermetallic layer decreased the bond strength on the SnInAg/Au/Ni/Cu interface. By using the pure creep test, the Arrhenius diagram of the Sn-15In-2.8Ag BGA assembly at a constant stress of 16 MPa consists of two straight lines intersecting at 50 °C. This result indicates that two kinds of creep mechanism controlled the Sn-15In-2.8Ag BGA assembly deformation under various homologous temperatures. The apparent activation energy for creep of the Sn-15In-2.8Ag BGA assembly at constant stress of 16 MPa at test temperatures higher than 50 °C was 24.3 kJ/mol. On the other hand, the creep voids could be nucleated at the $AuIn_2$ intermetallics and grain boundaries, which reduced the solder's cross-sectional area and led the Sn-15In-2.8Ag BGA assembly to fail rapidly with a transgranular creep fracture.

Acknowledgment

The authors would like to acknowledge the financial support of this work from the National Science Council of the Republic of China under grant no. NSC 91-2216-E-216-002.

References

1. S.K. Kang and A.K. Sarkhel, Lead (Pb)-Free Solders for Electronic Packaging, *J. Electron. Mater.*, 1994, **23**(8), p 701–707
2. M. McCormack, S. Jin, and G.W. Kammlott, Enhanced Solder Alloy Performance by Magnetic Dispersions, *IEEE Trans. Comp. Packaging Manuf. Technol. Part A*, 1994, **17**(3), p 452–457
3. M. Harada and R. Satoh, Mechanical Characteristics of 96.5Sn/3.5Ag Solder in Microbonding, *IEEE Trans. Comp. Hybrid Manuf. Technol.*, 1990, **13**(4), p 736–742
4. H. Mavoori, J. Chin, S. Vaynman, B. Moran, L. Keer, and M. Fine, Creep, Stress Relaxation, and Plastic Deformation in Sn-Ag and Sn-Zn Eutectic Solders, *J. Electron. Mater.*, 1997, **26**(7), p 783–790
5. A.M. Minor and J.W. Morris Jr., Growth of a Au-Ni-Sn Intermetallic Compound on the Solder-Substrate Interface after Aging, *Metall. Trans. A*, 2000, **31A**(3), p 798–800
6. G. Humpston and D.M. Jacobson, *Principles of Soldering and Brazing*, 1st ed., ASM International, Materials Park, OH, 1993, p 31–70
7. M.S. Yeh, Effects of Indium on the Mechanical Properties of Ternary Sn-In-Ag Solders, *Metall. Trans. A*, 2003, **34A**(2), p 361–365
8. M.D. Mathew, H. Yang, S. Movva, and K.L. Murty, Creep Deformation Characteristics of Tin and Tin-Based Electronic Solder Alloys, *Metall. Trans. A*, 2005, **36A**(1), p 99–105
9. R. Darveaux and K. Banerji, Constitutive Relations for Tin-Based Solder Joints, *IEEE Trans. Comp. Hybrid Manuf. Technol.*, 1992, **15**(6), p 1013–1024